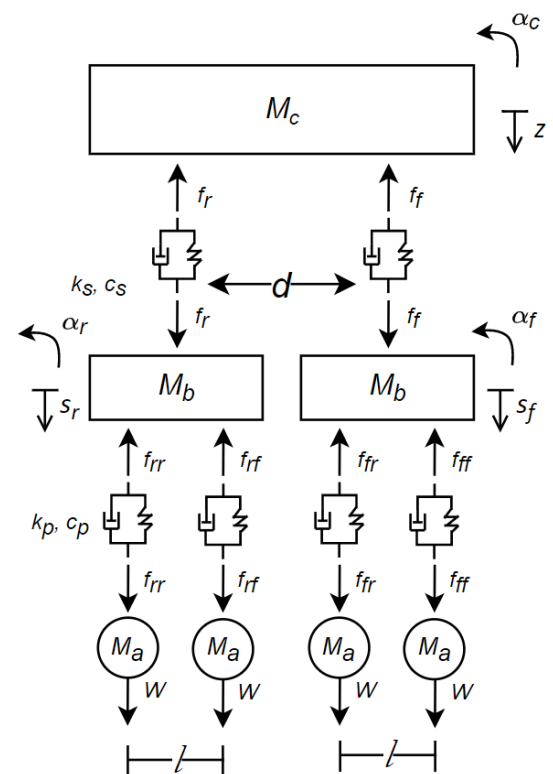
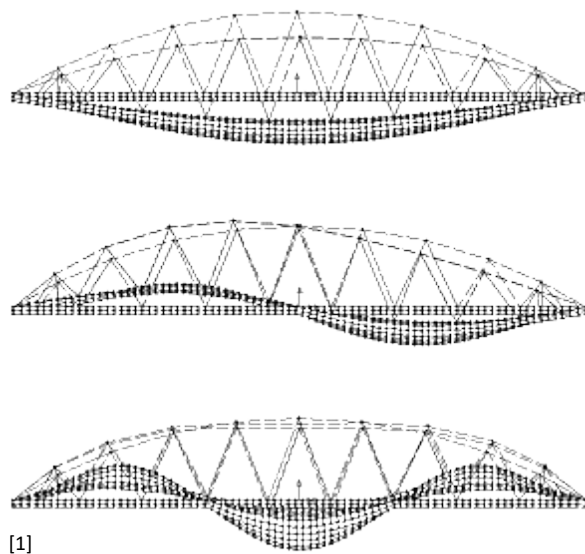


# The influence of train parameters on the train-bridge dynamic interaction



Willem Wolswijk

Supervisors: Yuanchen Zeng, Zili Li

June 2021

Bachelor's Final Project (BEP), TU Delft



## *Preface*

This research was conducted to fulfil the graduation requirements of the Bachelor of Civil Engineering at the Delft University of Technology. The research was conducted between April and June of 2021.

To consult the code used for this project, access the GitHub page through <https://github.com/WillemWolswijk/Train-bridge-Dynamic-Models.git>.

I would like to thank both of my supervisors for their outstanding support and guidance during this process. Their great approachability throughout the project stood out from other projects at the university. I look forward to further collaborations.

Furthermore, I would like to thank my family for their support and interest shown during the process. My parents deserve a special note of thanks for their kind and motivating words.

I hope you enjoy your reading.

Delft, June 2021

*Willem Wolswijk*

## *Summary*

In this paper, various two-dimensional (2D) models of train-bridge dynamic interaction are established using multibody dynamics theory and beam theory. The models are solved using the Newmark- $\beta$  method, a common implicit integration method for structural dynamics.

The research gives a description of the effect of train parameters on the train-bridge dynamics using a full 2D train model. By clearly describing the train and bridge models used, an attempt will be made to accurately describe the physics behind the models.

The result of the simulations describe the differences between different models, after which the effects of various train parameters on the midpoint displacements are illustrated.

## Table of Contents

Preface .....	i
Summary .....	ii
1. Introduction.....	1
1.1 Rationale .....	1
1.2 Literature review .....	1
1.3 Problem statement .....	2
1.4 Aims and objectives.....	2
1.5 Research questions and methods .....	2
1.6 Scope of the research .....	2
1.7 Organisation of the report .....	3
2. Theoretical Modelling .....	4
2.1 Modelling of a bridge .....	4
2.2 Modelling of a train.....	7
2.2.1 Moving point load model .....	8
2.2.2 Moving mass model .....	9
2.2.3 Moving spring-damping-mass model .....	10
2.2.4 Two-axle vehicle bridge model.....	12
2.2.5 Train-bridge dynamic interaction model.....	14
3. Numerical Simulations .....	17
3.1 Method.....	17
3.2 Analytical solution vs. Numerical solution .....	18
3.3 Comparison between different models.....	19
3.3.1 MCFM vs. MMM .....	19
3.3.2 MMM vs MSDMM.....	20
3.3.3 MSDMM vs TAVBM.....	21
3.3.4 TAVBM vs. TBDIM .....	22
3.4 Effect of train parameters.....	23
3.4.1 Effect of the vehicle speed.....	23
3.4.2 Effect of the vehicle mass.....	24
3.4.3 Effect of the suspension parameters.....	25
4. Conclusions and Discussions .....	27
References.....	28

## 1. Introduction

In this chapter, an overview of this research will be represented. Besides a short background on the topic, the layout of the report is presented.

### 1.1 Rationale

Due to the sustainability and capacity of train transport, the size of the train sector is continuously increasing (Eurostat, 2020).

The dynamic train-bridge interaction is a crucial aspect to bridge design, especially in high-speed and heavy railways. Running trains induce severe vibrations to the bridge causing changes to the substructure. In turn, the deflections in the beam create dynamic movements in the train. This can significantly influence the passenger comfort in the train.

### 1.2 Literature review

Due to its importance in train bridge design, the dynamic train-bridge interaction has been a topic of research for many decades.

The first known research was performed by Stokes who researched differential equations relating to the breaking of railway bridges because of the Dee Bridge disaster of 1847 (Stokes, 1849). Willis researched the effects caused by a moving weight over an elastic bar (Willis, 1849).

The Timoshenko analysed the resonance problem through harmonic forcing (Timoshenko, 1922) after which Jeffcot investigated the effects of the inertia of the train (Jeffcot, 1929). Biggs investigated the sprung model and proposed semi-analytical solutions to the models in his book 'Introduction to Structural Dynamics' (Biggs, 1964).

The dynamic response of beams traversed by two-axle loads was researched by Robert Wen who performed numerical analysis to obtain his results (Wen, 1960). A full train model was first established succeeding the development of the Finite Element Method (FEM) and was developed by many researchers.

A model in which the track was modelled separately from the bridge was first researched by Zhai who investigated the effects of different bridge and train parameters on the dynamic interaction (Zhai & Sun, A Detailed Model for Investigating Vertical Interaction between Railway Vehicle and Track, 1994). With the development of high-speed railways in China in the following years, the model was perfected (Zhai, Han, Chen, Ling, & Zhu, 2019).

Multiple studies have researched the effects of bridge and track properties on the dynamic interaction. For instance, the dynamic interaction between a train system and a cable bridge has been researched using a 3D model with 48 DOFs (Jalili & Orafa, 2014). The effects of wagon parameters, lateral position of the rails and rail irregularities were investigated. Furthermore, the effect of track irregularities and thermal deformation on the dynamic train-bridge interaction was researched using a model with 27 DOFs (Tian, Zhang, & Xia, 2016). Additionally, the effects of concrete shrinkage and creep on the dynamic interaction was researched (Chen & Han, 2017)

The response of the train-bridge system to external forces have also been extensively studied. For instance, the response of the train-bridge system to seismic action has also been examined (Xia & Liu, 2014). Crucially for bridge dynamics, the response of the train-track-bridge system to derailment impacts has also been examined (Ling, Dhanasekar, & Thambiratnam, 2017).

Furthermore, numerous studies have been performed to investigate the interaction between the bridge structure and the soil. The dynamic soil-structure interaction (SSI) has been researched using simple concepts from the finite element theory (Ülker-Kaustell, Karoumi, & Pacoste, 2010). The influence of the soil-structure interaction on the train-bridge system has also been examined (Li, Liu, Liu, & Zhang, 2013) and the direct effects of the soil stiffness on the bridge behaviour has been investigated too (Devesa, 2009).

Effects of bridge vibrations on the surrounding environment have been extensively studied. The ground vibrations due to trains over bridges have been examined (Wu & Yang, 2004). Furthermore, research has been done into building vibrations induced by the vehicle-bridge interaction (Zhu, Yu, Zhu, & Gao, 2013).

For the dynamic interaction of high-speed trains, research was performed using a train model with 27 DOFs (Zhang, Xia, & Guo, 2008).

Extensive research has been performed in the validation of numerical models. Experimental validation of a numerical 3D model has been performed by comparison with a small-scale model (Sneideris, Bucinska, Agapii, & Andersen, 2015). Numerical results have also been verified by field tests (Andersson & Karoumi, 2015).

### *1.3 Problem statement*

Due to the increasing demand for passenger rail transport, there is an increasing need for passenger comfort.

Furthermore, to accommodate the increasing demand of train transport, the capacity of the train system must be increased. To increase the capacity, larger and faster trains could be developed, influencing the train-bridge interaction and passenger comfort.

### *1.4 Aims and objectives*

This research aims to estimate the effects train parameters on the dynamics of the train-bridge system.

To properly discuss the influence of these characteristics, multiple train models will be developed, examined, and compared. The models that are considered will be of increasing complexity and validated through comparison of the results.

After the models have been developed, they will be solved through a numerical method and the results will be discussed. Through running various simulations with differing train parameters, the influence of the parameters will be illustrated.

### *1.5 Research questions and methods*

The methods used in this research will be quantitative. After creating the models through Newton's laws of motion, the equations of motion will be numerically solved. The numerical results will be compared between the models and discussed. The influence of various train parameters will be reported.

### *1.6 Scope of the research*

The models that will be developed will consist of the train modelled as a mass-spring-damper system while the track and bridge deck will be modelled together as a beam element. The bridge-track element will be modelled as a simply supported Euler-Bernoulli beam.

The models discussed in this research will remain 2D models. The models will be of a varying complexity and accuracy. It will start from a moving force model followed by a moving mass model. The spring-dampers dynamics will be introduced through the moving spring-damping-mass model. Beyond that, the

pitch of the vehicle will be considered using the two-axle vehicle bridge model followed by the full train-bridge dynamic interaction model.

### *1.7 Organisation of the report*

Chapter 2 of this report describes the modelling in this research. Beyond describing modelling of the bridge element, the different train models will be developed. Chapter 3 starts by describing the numerical methods used to obtain the results after which the results are presented. In Chapter 4 the results are discussed.

## 2. Theoretical Modelling

In this chapter, the modelling of the bridge and the train will be discussed. Firstly, the bridge modelling will be discussed in detail. Secondly, the train models will be developed, and the differential equations will be set up.

### 2.1 Modelling of a bridge

To accelerate the simulations and simplify the modelling procedure, the bridge deck is simplified together with the track.

The track-bridge element involved in the train-bridge dynamic interaction is simplified to a Euler-Bernoulli beam and thus does not consider the effects of shear deformation and rotational bending effects. This simplification results in the Euler-Bernoulli equation (Erochko, 2020):

$$M = -EI \frac{d^2w}{dx^2} \quad (2-1)$$

where  $EI$  is the bending stiffness of the beam,  $w$  is the displacement of the beam,  $x$  is the distance along the beam and  $M$  is the bending moment at location  $x$ .

Furthermore, the bridge is assumed to be simply supported at both ends of the bridge. The result is that at the ends of the beams, rotations are free and bending moments are zero.

Lastly, the beam cross-section is assumed to be homogenous; the cross-section does not change in the length of the bridge.

If no forces act on the beam, the vertical displacement of the beam can be expressed by the following equation of motion (EOM) (Biggs, 1964):

$$m\ddot{u} + c_e\dot{u} + Ic_i\dot{u}'''' + EIu'''' = 0 \quad (2-2)$$

where  $u$  is the vertical displacement as a function of time and the  $x$ -coordinate,  $m$  is the mass per unit length of the beam,  $c_e$  is the external damping coefficient,  $c_i$  is the internal damping coefficient,  $I$  is the second moment of inertia of the bridge and  $E$  is the elastic modulus of the bridge. An overdot ( $\dot{u}$ ) represents a first order derivative to time and an apostrophe ( $u'$ ) represents a first derivative to the position  $x$ .

However, upon modelling of the bridge it can be stated that the damping of the bridge itself can be neglected as it has little effect on the dynamics of the bridge (Yang, Yau, & Wu, 2004) (Majka & Hartnett, 2008). Thus, Eq. 2 can be simplified to:

$$m\ddot{u} + EIu'''' = 0 \quad (2-3)$$

If a point load acts on the beam, it introduces a term on the right-hand side of Eq. (2-3). For multiple discrete point loads, the EOM for the beam can be written as follows (Lorieux, 2008):

$$m\ddot{u} + EIu'''' = \sum_{j=1}^{N_{contact}} F_j(t) * \delta\left(x - v(t - t_j)\right) * \varepsilon_j(t) \quad (2-4)$$

where  $N_{contact}$  is the number of forces acting on the beam,  $F_j(t)$  is the force induced by the  $j$ th force,  $\delta$  is the Dirac delta function,  $v$  is the horizontal velocity of the loads,  $t_j$  is the entry time of the  $j$ th force and  $\varepsilon_j(t) = (Heaviside(t - t_j) - Heaviside(t - t_j - \frac{L}{v}))$  where  $L$  is the length of the beam. In the formula for  $\varepsilon_j(t)$ , the Heaviside function is defined such that:

$$Heaviside(s) = \begin{cases} 0, & s < 0 \\ 1, & s \geq 0 \end{cases} \quad (2-5)$$

It should be noted that although Eq. (2-4) only has one unknown ( $u$ ), but it is difficult to solve due to the derivatives to position  $x$  (4<sup>th</sup> order) and time  $t$  (2<sup>nd</sup> order). To tackle this issue, the separation of variables will be performed (Biggs, 1964). This will result in a solution made up of a time-dependent part and a mode shape:

$$u(x, t) = \sum_{n=1}^N \phi_n(x) * q_n(t) \quad (2-6)$$

where  $n$  is the order of beam mode,  $N$  is the total number of beam modes taken into consideration and  $q_n(t)$  represents the generalised coordinate for the  $n$ th mode. The mode shape  $\phi_n(x)$  depends on the boundary conditions of the bridge and has the general form written as

$$\phi_n(x) = A_n \sin(a_n x) + B_n \cos(a_n x) + C_n \sinh(a_n x) + D_n \cosh(a_n x) \quad (2-7)$$

For a simply supported beam, the following two boundary conditions are true: at the ends of the beam, there is no displacement ( $u = 0$ ) and there are no bending moments ( $M = 0$  or  $\frac{d^2 w}{dx^2} = 0$ ). Taking this into account, Eq. (2-7) can be simplified to

$$\phi_n(x) = \sin\left(\frac{n*\pi*x}{L}\right) \quad (2-8)$$

An illustration of the different beam modes described by Eq. (2-8) is shown in Figure 2-1.

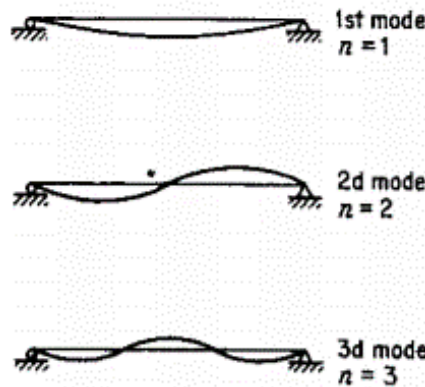


Figure 2-1: Beam modes for a simply supported beam (Biggs, 1964)

Using Eq. (2-6) and Eq. (2-8), the velocity and acceleration of the beam at any position  $x$  on the beam can be written as follows:

$$\frac{d}{dt} u(x, t) = \sum_{n=1}^N \sin\left(\frac{n*\pi*x}{L}\right) * \frac{d}{dt} q_n(t) \quad (2-9)$$

$$\frac{d^2}{dt^2} u(x, t) = \sum_{n=1}^N \sin\left(\frac{n*\pi*x}{L}\right) * \frac{d^2}{dt^2} q_n(t) \quad (2-10)$$

To solve the generalised coordinate  $q_n(t)$  for every beam mode, Eq. (2-4) is often rewritten using the properties described by Eq. (2-6) and Eq. (2-8) (Frýba, 1972):

$$\frac{d^2}{dt^2} q_n(t) + \omega_n^2 * q_n(t) = \frac{2}{L*m} \sum_{j=1}^{N_{contact}} F_j(t) * \phi_n(v * (t - t_j)) * \varepsilon_j(t) \quad (2-11)$$

where  $\phi_n$  is described by Eq. (2-8) and  $\omega_n$  is the natural frequency of the beam mode as defined by Eq. (2-12):

$$\omega_n = \sqrt{\frac{EI \cdot \pi^4 \cdot n^4}{m \cdot L^4}} \quad (2-12)$$

It should be noted that Eq. (2-11) must be solved for all the beam modes  $1..N$  and summed according to Eq. (2-6) to obtain the total displacement.

The parameters used for the modelling of the bridge are based on the Skidträsk Bridge in Sweden which is commonly used to analyse structural dynamics of bridges. The parameters used for this research are listed in Table 1.

<b>Data</b>	<b>Symbol</b>	<b>Unit</b>	<b>Value</b>
Span	$L$	m	36
Elastic modulus	$E$	N/m <sup>2</sup>	$2.1 \cdot 10^{11}$
Second moment of area	$I$	m <sup>4</sup>	0.41
Mass per unit length	$m$	kg/m	17,000

*Table 1: Parameters for the beam based on the Skidträsk Bridge (Cantero, Karoumi, & Ülker-Kaustell, 2016)*

A common velocity for a passenger train over the Skidträsk Bridge is  $v = 100 \text{ km/h} = 27.78 \text{ m/s}$  (Lorieux, 2008). Therefore this speed is selected for the modelling.

## 2.2 Modelling of a train

The modelling of a train moving along a simply supported beam can be performed with vastly increasing complexity. This chapter will start with the simplest model, the moving point load, after which the complexity is gradually increased. For all models, it is assumed that contact is never lost between the train's wheels and the bridge.

Parameters of the train such as masses, spring stiffnesses and dimensions are based on the Mark 4 Carriage, a passenger train in the UK. The parameters used in this research are given in Table 2.

Data	Symbol	Unit	Value
<i>Mass properties</i>			
Mass of the car body	$M_c$	kg	$42.11 \cdot 10^3$
Inertial moment for the pitch motion of the car body	$I_c$	$\text{kg} \cdot \text{m}^2$	$18.30 \cdot 10^5$
Mass of a bogie	$M_b$	kg	$68.20 \cdot 10^2$
Inertial moment for the pitch motion of a bogie	$I_b$	$\text{kg} \cdot \text{m}^2$	$52.57 \cdot 10^2$
Mass of a wheelset	$M_a$	kg	$18.13 \cdot 10^2$
<i>Suspension stiffnesses</i>			
Primary suspension (vertical)	$k_p$	N/m	$31.85 \cdot 10^5$
Secondary suspension (vertical)	$k_s$	N/m	$5.66 \cdot 10^5$
<i>Suspension damping</i>			
Primary suspension (vertical)	$c_p$	$\text{N} \cdot \text{s}/\text{m}$	$32.41 \cdot 10^3$
Secondary suspension (vertical)	$c_s$	$\text{N} \cdot \text{s}/\text{m}$	$26.24 \cdot 10^3$
<i>Dimensions</i>			
Inter-wheelset distance	$l$	m	2.5
Inter-bogie distance	$d$	m	16

Table 2: Train carriage parameters (Majka & Hartnett, 2008)

The different train models that are discussed are illustrated below.

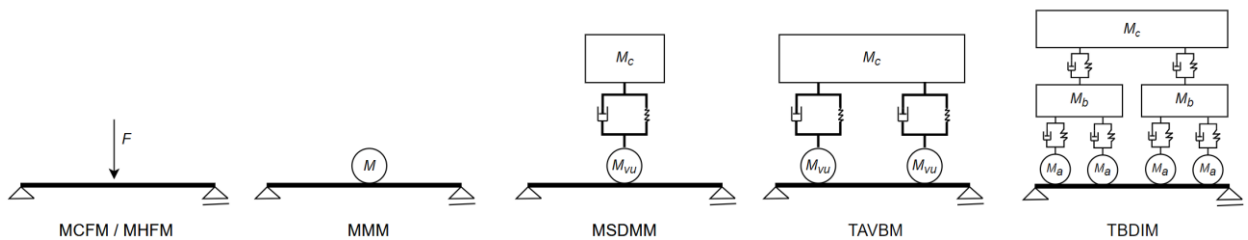


Figure 2-2: An overview of the train models

### 2.2.1 Moving point load model

The moving point load model is the simplest and earliest model to describe bridge dynamics under moving loads. It achieves simple but inaccurate solutions, as the model does not consider the train-bridge dynamic interaction. Furthermore, it does not consider the inertia of the train.

The moving point load model consists of a force moving along the beam at a constant speed (Figure 2-3). The moving train can either be modelled by a constant force in a Moving Constant Force Model (MCFM) or by a harmonic force in a Moving Harmonic Force Model (MHFM).

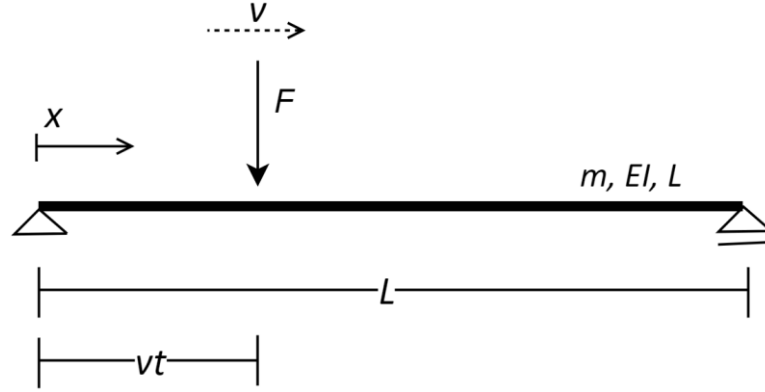


Figure 2-3: The moving force model

The equation of motion for the beam traversed by a point load is constructed using Eq. (2-4). For the case of a single point load,  $N_{contact} = 1$  with  $t_1 = 0$  and  $F_1(t) = F(t)$ . Simplifying this equation results in

$$m\ddot{u} + EIu'''' = F(t) * \delta(x - vt) \quad (2-13)$$

where  $F(t)$  is the contact force between the train and the beam. To solve for the generalized coordinates  $q_1(t), \dots, q_N(t)$ , Eq. (2-11) will be used. This results in

$$\frac{d^2}{dt^2} q_n(t) + \omega_n^2 * q_n(t) = \frac{2}{L*m} * F(t) * \phi_n(v * t) \quad (2-14)$$

where  $\phi_n(v * t)$  is the beam mode shape at the position of the load, defined as

$$\phi_n(v * t) = \sin\left(\frac{n*\pi*v*t}{L}\right) \quad (2-15)$$

The contact force  $F(t)$  can be defined as  $F(t) = p$  for a constant force and  $F(t) = p * (1 + A \sin(\omega * t))$  for a harmonic force where  $\omega$  is the forcing frequency and  $A$  is the amplitude of the harmonic force. The force  $p$  is the weight of the vehicle defined as:

$$p = g * (M_c + 2 * M_b + 4 * M_a) \quad (2-16)$$

where  $g$  is the acceleration due to gravity.

### 2.2.2 Moving mass model

The moving mass model consist of a mass moving over the beam at a constant speed (Figure 2-4). The assumption made in this simplification is that the displacement of the train is equal to that of the beam at the location of the mass. Furthermore, it is assumed that the primary and secondary springs and dampers are infinitely stiff. As a result, the mass  $M$  of the moving mass is the total mass of the train carriage consisting of the car body, two bogies and four wheelsets:

$$M = M_c + 2 * M_b + 4 * M_a \quad (2-17)$$

The increased model complexity with regards to the MCFM originates from the inclusion of the inertia of the mass.

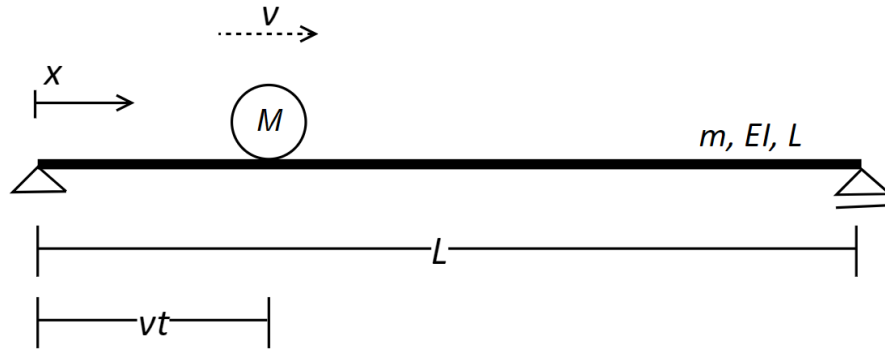


Figure 2-4: The moving mass model

The equation of motion for this system can be created using Eq. (2-11). Like the MCFM model,  $N_{contact} = 1$  with  $t_1 = 0$ . For this model, the force  $F_1(t)$  can be defined as follows:

$$F_1(t) = M * g - M * \ddot{u}_v \quad (2-18)$$

The variable  $u_v$  is the displacement of the beam at the location of the rolling mass, as described below.

$$u_v = u(vt, t) = \sum_{n=1}^N \sin\left(\frac{n\pi vt}{L}\right) * q_n(t) \quad (2-19)$$

Using Eq. (2-11) and Eq. (2-18), the equation of motion for the beam can be found as

$$\frac{d^2}{dt^2} q_n(t) + \omega_n^2 * q_n(t) = \frac{2}{L * m} * (M * g - M * \ddot{u}_v) * \phi_n(v * t) \quad (2-20)$$

In this model, the generalised coordinates  $q_1(t), \dots, q_N(t)$  are coupled to one another: the equation for any generalised coordinate  $q_n(t)$  contains references to the other generalised coordinates. Therefore, the results are dependant of one another and all  $N$  equations must be solved in conjunction with one another.

### 2.2.3 Moving spring-damping-mass model

The moving spring-damping-mass model (MSDMM) consists of a mass sprung above another mass as shown in Figure 2-5. The train model consists of 1 DOF (ignoring the DOF of the lower mass): the displacement  $z$ . In relation to a train,  $M_c$  refers to the train body and  $M_{vu}$  refers to a combined mass of 2 bogies and 4 wheelsets.

The spring and damper system between the upper and the lower mass refers to the secondary suspension, which is typically less stiff than the primary suspension.

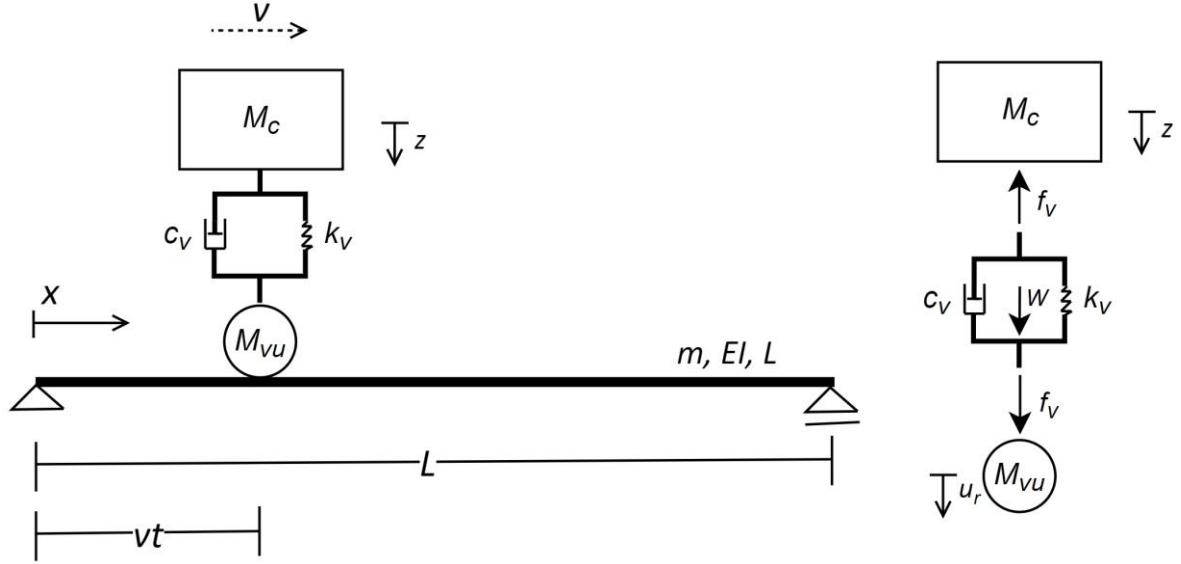


Figure 2-5: The sprung mass system (left) and the sprung mass train model (right)

To retrieve the equations of motion for this system, Eq. (2-11) will be used again. To obtain the EOMs for this system, it is useful to define the interaction forces between the elements. The interactive force  $f_v$  and weight component  $W$  can be defined as follows:

$$f_v = k_v * (z - u_v) + c_v * (\dot{z} - \dot{u}_v) \quad (2-21)$$

$$W = M_c * g \quad (2-22)$$

where  $c_v$  is the damping coefficient,  $k_v$  is the spring stiffness,  $u_v$  is the beam displacement at the sprung mass location and  $z$  is the displacement of the upper mass with respect to its equilibrium position.

As stated, the spring-damper system refers to the secondary suspension. Given that there are four spring-damper systems per train carriage, we define  $k_v$  and  $c_v$  as  $k_v = 4k_s$  and  $c_v = 4c_s$ .

Using the interaction force defined by Eq. (2-21) and the weight component defined by Eq. (2-22), the equation of the beam can be determined using Eq. (2-11). Like the MCFM and MMM,  $N_{contact} = 1$  with  $t_1 = 0$ . The force  $F_1(t)$  can be defined as

$$F_1(t) = M_{vu} * (g - \ddot{u}_v) + f_v + W \quad (2-23)$$

where  $M_{vu}$  is the mass of the lower mass object and can be defined as  $M_{vu} = 2 * M_b + 4 * M_a$ . Substituting the contact force into Eq. (2-11) yields the following equation:

$$\frac{d^2}{dt^2} q_n(t) + \omega_n^2 * q_n(t) = \frac{2}{L * m} * (M_{vu} * (g - \ddot{u}_v) + f_v + W) * \phi_n(v * t) \quad (2-24)$$

As shown in Figure 2-5, the weight component  $W$  of the upper mass  $M_c$  is assumed to act directly onto the beam and not through forcing onto the upper mass. This assumes that the system is in an equilibrium state as it enters the beam.

To prove this assumption is accurate, we can imagine a simple sprung mass system defined by the following equations:

$$-k * (z' - u_v) + M_c * g = M_c * \ddot{z}' \quad (2-25)$$

$$k * (z' - u_v) = M_{vu} * (g - \ddot{u}_v) \quad (2-26)$$

where  $z'$  is the displacement from a random position such that the system is not in equilibrium. Let us define the displacement as  $z' = z_e + z$  where  $z_e$  is the equilibrium position with respect to  $z'$  and  $z$  is the displacement with respect to the equilibrium position. Through simplifying, we obtain

$$M_c * g = k * z_e \quad (2-27)$$

which results in:

$$k * (z - u_v) + M_c * g = M_{vu} * (g - \ddot{u}_v) \quad (2-28)$$

Since the differential equations assume the system to be in an equilibrium position prior to entering the beam, the weight of the upper mass  $M_c$  can act directly onto the beam.

Because the Eq. (2-24) contains two unknowns ( $z$  and  $u$ ) we cannot find the solution yet. To find the solution, another equation of motion is needed which refers to the equilibrium of forces for the sprung mass:

$$-f_v = M_c * \ddot{z} \quad (2-29)$$

Like the moving mass model, the beam modes are coupled to one another through the beam equations and must therefore be solved simultaneously.

### 2.2.4 Two-axle vehicle bridge model

The two-axle vehicle bridge model (TAVBM) is of higher complexity as the train model consists of 2 DOFs (ignoring the DOFs of the lower masses). It consists of an upper mass sprung onto two lower masses as shown in Figure 2-6.

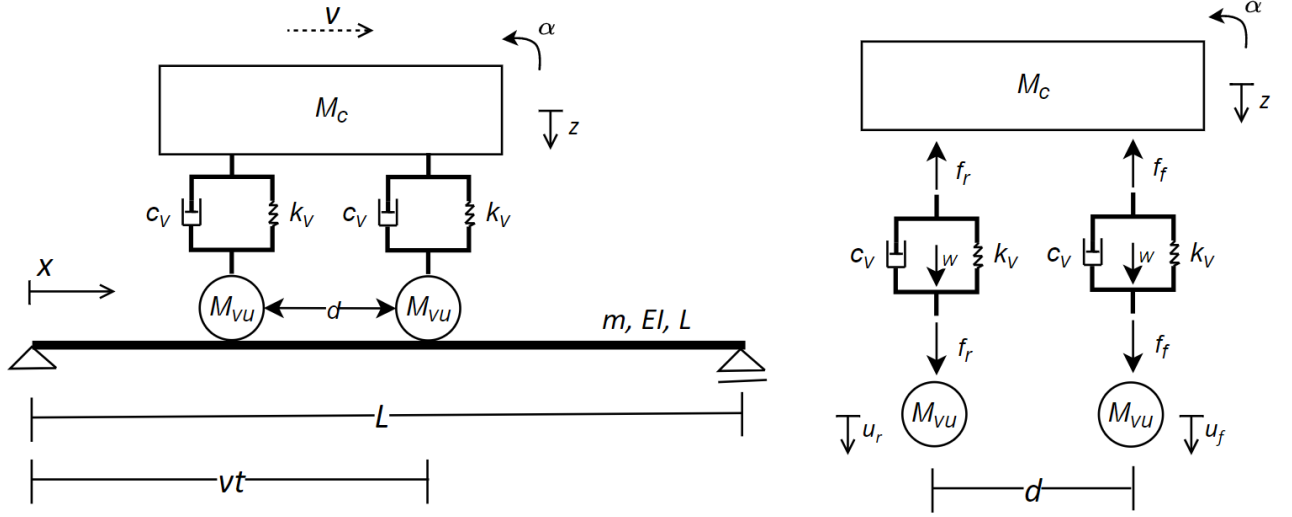


Figure 2-6: TAVBM model system (left) and the train model (right)

In this model, only the secondary suspension is considered. The spring and damper system, indicated with the coefficients  $k_v$  and  $c_v$ , therefore connects the car body  $M_C$  with the bogies  $M_{vu}$ . In the bogie mass  $M_{vu}$ , the wheelset masses are included such that

$$M_{vu} = M_b + 2 * M_a$$

Given that there are 2 sets of spring-dampers systems per bogie, the spring stiffness and damper coefficients  $k_v$  and  $c_v$  are defined as  $k_v = 2k_s$  and  $c_v = 2c_s$ .

To set up the equations of motion, the interactive forces between the car body and the bogies are described:

$$f_r = k_v \left( z(t) - u_{rear} + \frac{d}{2} * \alpha(t) \right) + c_v \left( \dot{z}(t) - \dot{u}_{rear} + \frac{d}{2} * \dot{\alpha}(t) \right) \quad (2-30)$$

$$f_f = k_v \left( z(t) - u_{front} - \frac{d}{2} * \alpha(t) \right) + c_v \left( \dot{z}(t) - \dot{u}_{front} - \frac{d}{2} * \dot{\alpha}(t) \right) \quad (2-31)$$

where  $\alpha(t)$  is the pitch of the car body,  $z(t)$  is the displacement of the car body and  $u_{rear}$  and  $u_{front}$  are the displacements of the rear and front bogies, respectively.

Like the MSDMM, the weight component of the sprung mass is modelled to act directly onto the beam. This weight component  $W$  can be defined as

$$W = \frac{1}{2} M_c. \quad (2-32)$$

The increased complexity of this model stems from the additional DOFs and the dual contact points between the model and the beam. To formulate the equation of motion for the beam, Eq. (2-11) is applied. For this model  $N_{contact} = 2$ ,  $t_1 = 0$ ,  $t_2 = \frac{d}{v}$  and the contact forces  $F_1(t)$  and  $F_2(t)$  are defined as

$$F_1(t) = M_{vu}(g - \ddot{u}_{front}) + f_f + W \quad (2-33)$$

$$F_2(t) = M_{vu}(g - \ddot{u}_{rear}) + f_r + W \quad (2-34)$$

Note that since the wheels are assumed to move in conjunction with the beam, the wheel's displacements are defined as follows:

$$u_{rear} = \sum_{n=1}^N \sin\left(\frac{n\pi v(t-t_2)}{L}\right) * q_n(t) \quad (2-35)$$

$$u_{front} = \sum_{n=1}^N \sin\left(\frac{n\pi v(t-t_1)}{L}\right) * q_n(t) \quad (2-36)$$

Substituting the contact forces into Eq. (2-11) results in the following equation of motion for the generalised coordinate  $q_n(t)$ :

$$\frac{d^2}{dt^2} q_n(t) + \omega_n^2 * q_n(t) = \frac{2}{L*m} * (F_1(t) * \phi_n(v * t) * \varepsilon_1(t) + F_2(t) * \phi_n\left(v * \left(t - \frac{d}{v}\right)\right) * \varepsilon_2(t)) \quad (2-37)$$

where  $\varepsilon_1(t)$  and  $\varepsilon_2(t)$  are as defined in Chapter 2.1.

The remaining equations of motion must be derived from the vertical force equilibrium and rotational equilibrium of the sprung mass  $M_c$ :

$$-(f_r + f_f) = M_c * \ddot{z} \quad (2-38)$$

$$\frac{d}{2} * (f_f - f_r) = I_c * \ddot{\alpha} \quad (2-39)$$

Like the MMM of Chapter 2.2.2 and the MSDMM of Chapter 2.2.3, the generalised coordinates  $q_1(t), \dots, q_N(t)$  are coupled to one another. Consequentially, all equations of motion must be solved in conjunction with one another.

### 2.2.5 Train-bridge dynamic interaction model

The train-bridge dynamic interaction model (TBDIM) consists of a full 2D train model with one train car body, two bogies, and four wheelsets (Figure 2-7). The train model consist of 6 DOFs (ignoring the DOFs of the wheelsets). In contrast to the previous models, the TBDIM takes the dynamic influence of the primary suspension into account.

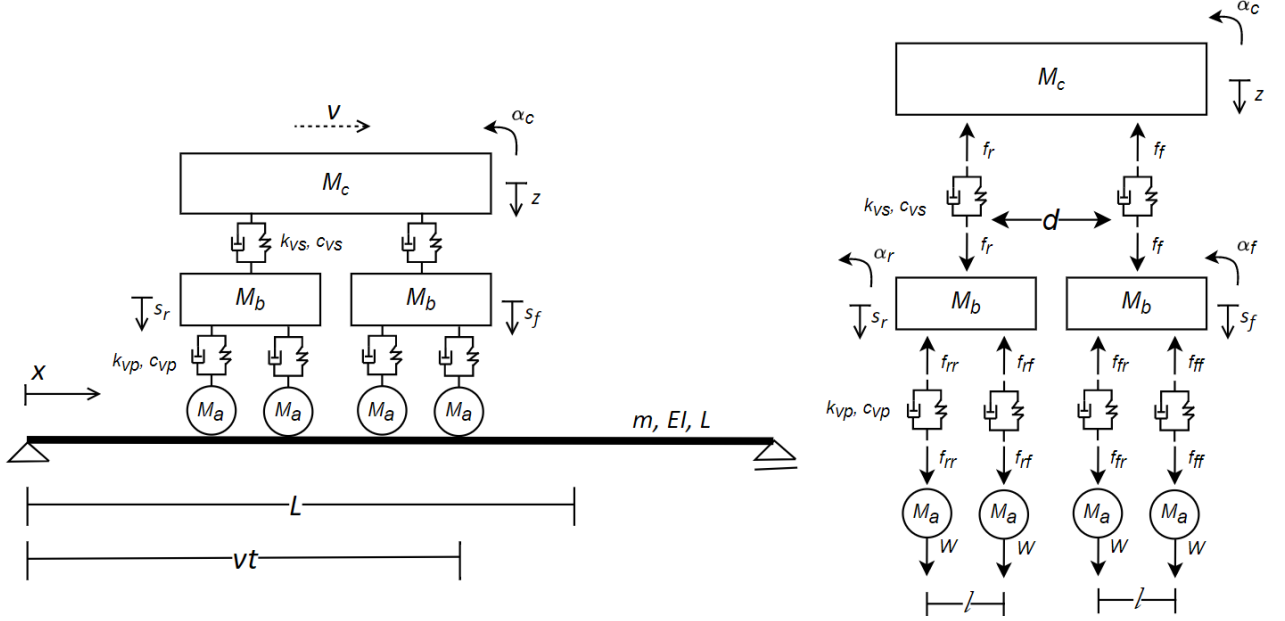


Figure 2-7: TBDIM model system (left) and the train model (right)

As seen in Figure 2-7, it is assumed the car body has two bogies with two wheelsets each. The subscripts  $r$  and  $f$  refer to rear and front bogies, respectively. To refer to the wheelsets, a double notation subscript is used in which the first letter refers to the bogie it is connected to, and the second letter refers to the location on the bogie (Table 3).

Rear bogie				Front bogie					
Displacement		Pitch		Displacement		Pitch			
$s_r$		$\alpha_r$		$s_f$		$\alpha_f$			
<b>Rear rear wheelset (axle 4)</b>				<b>Rear front wheelset (axle 3)</b>		<b>Front rear wheelset (axle 2)</b>		<b>Front front wheelset (axle 1)</b>	
Displacement	Entry time	Displacement	Entry time	Displacement	Entry time	Displacement	Entry time	Displacement	Entry time
$u_{rr}$	$t_4$	$u_{rf}$	$t_3$	$u_{fr}$	$t_2$	$u_{ff}$	$t_1$		0
	$(l+d)/v$		$d/v$		$l/v$				

Table 3: Notation for the bogies and wheelsets of the TBDIM model

To easily formulate the equations of motion, the interaction forces are determined. The notation corresponds with Figure 2-7 and Table 3. The interaction forces between the bogies and the car body can be written as

$$f_r = k_{vs} \left( z(t) - s_r(t) + \frac{d}{2} * \alpha_c(t) \right) + c_{vs} \left( \dot{z}(t) - \dot{s}_r(t) + \frac{d}{2} * \dot{\alpha}_c(t) \right) \quad (2-40)$$

$$f_f = k_{vs} \left( z(t) - s_f(t) - \frac{d}{2} * \alpha_c(t) \right) + c_{vs} \left( \dot{z}(t) - \dot{s}_f(t) - \frac{d}{2} * \dot{\alpha}_c(t) \right) \quad (2-41)$$

where  $z(t)$  is the displacement of the car body mass,  $\alpha_c(t)$  is the pitch of the car body,  $k_{vs}$  and  $c_{vs}$  are the secondary spring and dampers constants and  $s_f(t)$  and  $s_r(t)$  are as defined in Table 3.

Given that there are two secondary spring-damper systems for every bogie,  $k_{vS}$  and  $c_{vS}$  are defined as  $k_{vS} = 2k_s$  and  $c_{vS} = 2c_s$ .

The interaction forces between the bogies and wheelsets can also be determined:

$$f_{rr} = k_{vp} \left( s_r(t) - u_{rr} + \frac{d}{2} * \alpha_r(t) \right) + c_{vp} \left( \dot{s}_r(t) - \dot{u}_{rr} + \frac{d}{2} * \dot{\alpha}_r(t) \right) \quad (2-42)$$

$$f_{rf} = k_{vp} \left( s_r(t) - u_{rf} - \frac{d}{2} * \alpha_r(t) \right) + c_{vp} \left( \dot{s}_r(t) - \dot{u}_{rf} - \frac{d}{2} * \dot{\alpha}_r(t) \right) \quad (2-43)$$

$$f_{fr} = k_{vp} \left( s_f(t) - u_{fr} + \frac{d}{2} * \alpha_f(t) \right) + c_{vp} \left( \dot{s}_f(t) - \dot{u}_{fr} + \frac{d}{2} * \dot{\alpha}_f(t) \right) \quad (2-44)$$

$$f_{ff} = k_{vp} \left( s_f(t) - u_{ff} - \frac{d}{2} * \alpha_f(t) \right) + c_{vp} \left( \dot{s}_f(t) - \dot{u}_{ff} - \frac{d}{2} * \dot{\alpha}_f(t) \right) \quad (2-45)$$

where the variables  $u_{rr}$ ,  $u_{rf}$ ,  $u_{fr}$ ,  $u_{ff}$ ,  $\alpha_r$  and  $\alpha_f$  are as defined in Table 3,  $k_{vp}$  is the primary spring stiffness and  $c_{vp}$  is the primary damping coefficient.

Given that there are two primary spring-damper systems for every axle,  $k_{vp}$  and  $c_{vp}$  are defined as  $k_{vp} = 2k_p$  and  $c_{vp} = 2c_p$  where  $k_p$  and  $c_p$  are defined by Table 2.

Like the MSDMM of Chapter 2.2.3, the weight of the bogies and the car body are modelled to act directly onto the wheels to simulate an equilibrium state as the wheels enter the bridge. The weights are equally distributed with a contribution of  $W$  per wheel:

$$W = \frac{1}{4} M_c g + \frac{1}{2} M_b g. \quad (2-46)$$

The equations for the generalised coordinates  $q_1(t), \dots, q_N(t)$  must be set up using Eq. (2-11). For this train model,  $N_{contact} = 4$  with the entry times  $t_1, t_2, t_3$  and  $t_4$  as defined in Table 3. Using the interaction forces defined above, the contact forces  $F_1(t), F_2(t), F_3(t)$  and  $F_4(t)$  between the wheelsets and the beam can be determined:

$$F_1 = M_a(g - \ddot{u}_{ff}) + f_{ff} + W \quad (2-47)$$

$$F_2 = M_a(g - \ddot{u}_{fr}) + f_{fr} + W \quad (2-48)$$

$$F_3 = M_a(g - \ddot{u}_{rf}) + f_{rf} + W \quad (2-49)$$

$$F_4 = M_a(g - \ddot{u}_{rr}) + f_{rr} + W. \quad (2-50)$$

Like the previous models, the wheels are assumed to move in conjunction with the beam. Using Eq. (2-6), the wheel displacements can be calculated as follows:

$$u_{ff} = \sum_{n=1}^N \sin\left(\frac{n*\pi*v*(t-t_1)}{L}\right) * q_n(t) \quad (2-51)$$

$$u_{rf} = \sum_{n=1}^N \sin\left(\frac{n*\pi*v*(t-t_3)}{L}\right) * q_n(t) \quad (2-52)$$

$$u_{fr} = \sum_{n=1}^N \sin\left(\frac{n*\pi*v*(t-t_2)}{L}\right) * q_n(t) \quad (2-53)$$

$$u_{rr} = \sum_{n=1}^N \sin\left(\frac{n*\pi*v*(t-t_4)}{L}\right) * q_n(t). \quad (2-54)$$

The remaining six equations of motion refer to the vertical force equilibrium of the car body and of the bogies. These can be formulated using the interactive forces as described above:

$$-(f_r + f_f) = M_c * \ddot{z} \quad (2-55)$$

$$\frac{d}{2} * (f_f - f_r) = I_c * \ddot{\alpha}_c \quad (2-56)$$

$$f_r - (f_{rr} + f_{rf}) = M_b * \ddot{s}_r \quad (2-57)$$

$$\frac{l}{2} * (f_{rf} - f_{rr}) = I_b * \ddot{\alpha}_r \quad (2-58)$$

$$f_f - (f_{fr} + f_{ff}) = M_b * \ddot{s}_f \quad (2-59)$$

$$\frac{l}{2} * (f_{ff} - f_{fr}) = I_b * \ddot{\alpha}_f. \quad (2-60)$$

Like previous models, the generalised coordinates  $q_1(t), \dots, q_n(t)$  are coupled to one another: the solution to one of the variables is dependent on the solution of the other variables. Due to this, all equations must be solved simultaneously.

### 3. Numerical Simulations

In this chapter, the results of the numerical methods will be presented. Beyond comparing the results between different models, the effects of different train parameters are described.

To fully grasp the methods used to find the numerical solutions, the corresponding GitHub page can be consulted which contains all Maple code files for the models discussed in Chapter 2.2 (Wolswijk, 2021).

#### 3.1 Newmark- $\beta$ Method

From the systems described above, only the moving point load model can yield an analytical solution. For the other systems, the analytical solution cannot be found easily and therefore numerical methods must be applied to obtain results.

In the field of train-bridge dynamics, the Newmark- $\beta$  method is often used to perform implicit time integration. It is commonly used due to its unconditional stability and its flexibility, which was important in this research due to the range of models simulated (Newmark & Chan, 1952).

The Newmark-beta time integration method is used to solve an equation as described by Eq. (3-1). The coefficients  $\mathbf{M}$ ,  $\mathbf{C}$  and  $\mathbf{K}$  are matrices that describe the train-bridge dynamic system.

$$\mathbf{M}\ddot{u} + \mathbf{C}\dot{u} + \mathbf{K}u = f \quad (3-1)$$

where vector  $u$  is the unknown to be solved in this equation. The shape of the  $u$  vector depends on the DOFs of the model and on the number of beam modes that are calculated. For the TBDIM of Chapter 2.2.5, the  $u$  vector is as follows:

$$u = [q_1 \quad \dots \quad q_N \quad z \quad \alpha_c \quad s_b \quad \alpha_b \quad s_f \quad \alpha_f]^T \quad (3-2)$$

As can be seen, the size of the vector is  $N + 6$  by 1, where  $N$  is the number of beam modes that are taken into account. As such, the mass matrix  $\mathbf{M}$ , damping matrix  $\mathbf{C}$  and stiffness matrix  $\mathbf{K}$  all have the size  $N + 6$  by  $N + 6$  for the TBDIM.

The forcing vector  $f$  describes the external forcing on each element in the system. It is the same size as the  $u$  vector.

The Newmark-beta method solution can be obtained by following the steps outlined below (Maghdid, 2002):

1. Determine the integration parameters  $\beta$  and  $\gamma$  and the time step  $\Delta t$ . Recommended integration parameters are  $\beta = 0.25$  and  $\gamma = 0.5$  which provide unconditional stability.
2. Calculate the integration constants:

$$\begin{aligned} a_0 &= \frac{1}{\beta\Delta t^2}, & a_1 &= \frac{\gamma}{\beta\Delta t}, & a_2 &= \frac{1}{\beta\Delta t}, & a_3 &= \frac{1}{2\beta} - 1, \\ a_4 &= \frac{\gamma}{\beta} - 1, & a_5 &= \frac{\Delta t}{2} \left( \frac{\gamma}{\beta} - 2 \right), & a_6 &= \Delta t(1 - \gamma), & a_7 &= \gamma\Delta t. \end{aligned} \quad (3-3)$$

3. Define the  $\mathbf{M}$ ,  $\mathbf{C}$  and  $\mathbf{K}$  matrices and the  $f$  vector at time  $t_{n+1} = t_n + \Delta t$ .
4. Calculate the effective stiffness matrix at  $t_{n+1}$ :

$$\mathbf{K}_{eff} = \mathbf{K} + a_0\mathbf{M} + a_1\mathbf{C} \quad (3-4)$$

5. Calculate the effective forcing vector at  $t_{n+1}$ :

$$f_{eff\ t_{n+1}} = f_{t_{n+1}} + \mathbf{M}(a_0 u(t_n) + a_2 \dot{u}(t_n) + a_3 \ddot{u}(t_n)) + \mathbf{C}(a_1 u(t_n) + a_4 \dot{u}(t_n) + a_5 \ddot{u}(t_n)) \quad (3-5)$$

6. Calculate the deflections at time  $t_{n+1}$ :

$$u(t_{n+1}) = \mathbf{K}_{eff}^{-1} \cdot f_{eff\ t_{n+1}} \quad (3-6)$$

7. Calculate accelerations and velocities at time  $t_{n+1}$ :

$$\ddot{u}(t_{n+1}) = a_0(u(t_{n+1}) - u(t_n)) - a_2 \dot{u}(t_n) - a_3 \ddot{u}(t_n) \quad (3-7)$$

$$\dot{u}(t_{n+1}) = \dot{u}(t_n) + a_6 \ddot{u}(t_n) + a_7 \ddot{u}(t_{n+1}) \quad (3-8)$$

Steps 2 to 7 are repeated for the number of timesteps needed.

### 3.2 Analytical solution vs. Numerical solution

To ensure the accuracy of the numerical method, it should be compared to the analytical results. From the models that are discussed in this research, the analytical solution can only be calculated for the (constant and harmonic) moving force models.

To evaluate the accuracy of the numerical method, the numerical solutions of the MCFM and MHFM of Chapter 2.2.1 must be compared to their analytical solution. Specifically, the midpoint displacement is simulated and compared.

Figure 3-1 displays the comparison between the numerical solution and the analytical solution of the MCFM.

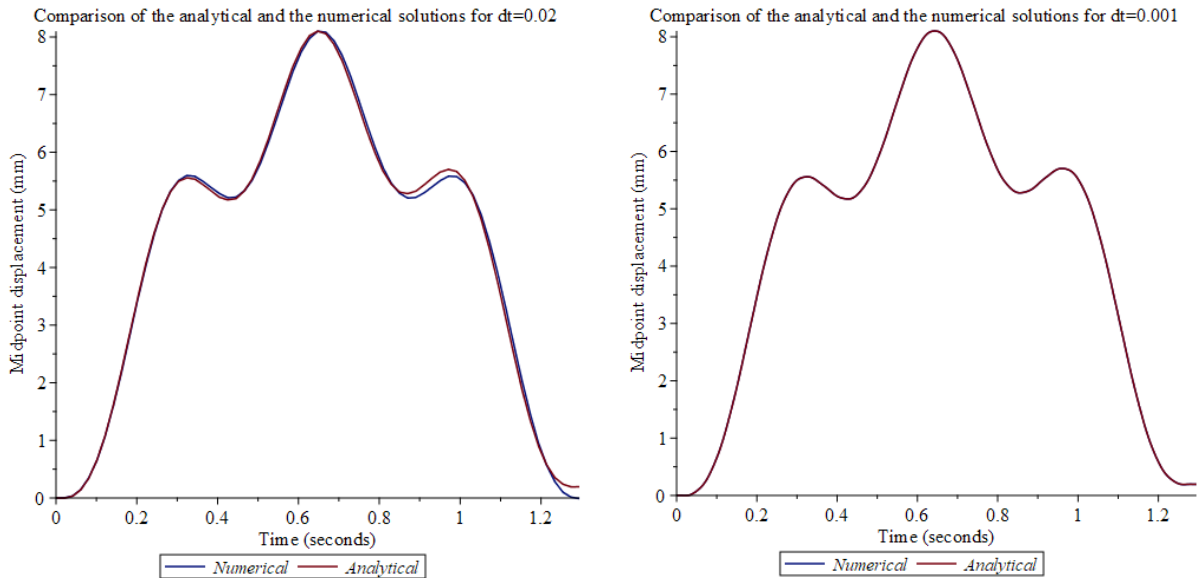


Figure 3-1: Effects of the timestep on the accuracy of the numerical solution using the MCFM model. High timestep (left) and low timestep (right).

To obtain the results for the MHFM models, the amplitude and frequency of the harmonic forcing must be defined. The amplitude is assumed to be  $A = 0.25$  and the forcing frequency  $\omega = 5 * \omega_n$  where  $\omega_n$  is the natural frequency of the beam as defined by Eq. (2-12). Note there is no physical reason behind these values; they are simply to illustrate comparison at hand.

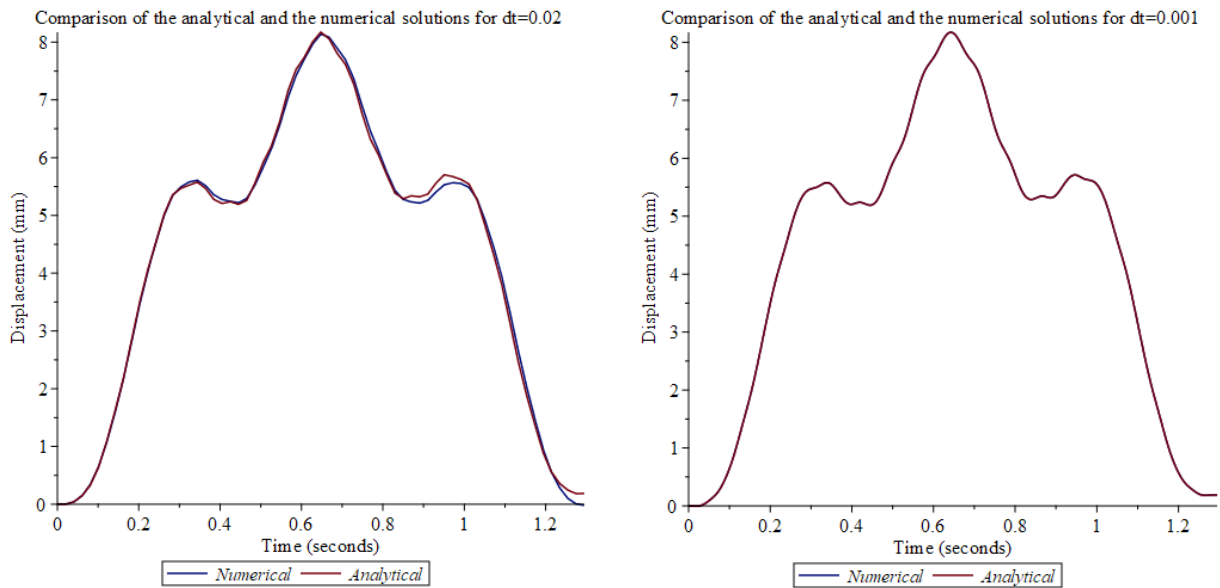


Figure 3-2: Effects of the timestep on the accuracy of the numerical solution using the MHFM model. High timestep (left) and low timestep (right).

The data from both the comparison using the MCFM and that using the MHFM confirm the accuracy of the numerical solution. Furthermore, it is shown that as  $\Delta t$  approaches zero the numerical solution approaches the analytical solution.

### 3.3 Comparison between different models

To validate the results of complex models, they should be compared to the results found in simpler models. This is performed by comparing every model to another model that is lightly less complex.

#### 3.3.1 MCFM vs. MMM

The difference in modelling between the MCFM and the MMM is the inclusion of inertia of the train. In the solution method there is a significant increase in complexity due to the coupling of modes (as explained in Chapter 2.2.2).

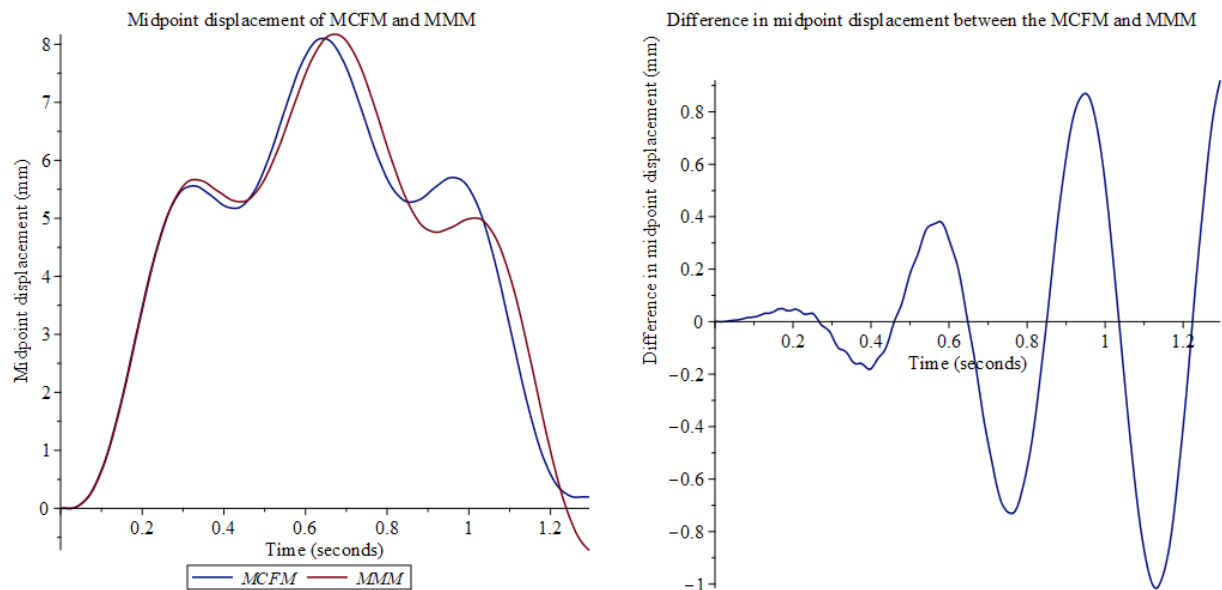


Figure 3-3: Comparison between the MCFM and MMM results. Midpoint displacements (right) and difference in midpoint displacement (left).

The left image of Figure 3-3 indicates that the midpoint displacement of the MCFM and the MMM follow similar trajectories. The maximum displacement is indifferent between the models.

The image on the right of Figure 3-3 confirms an effect that can be seen in the left image: the difference between the midpoint displacement of the different models increases as the point load/mass moves along the beam.

### 3.3.2 MMM vs MSDMM

The difference between the MMM and the MSDMM is the addition of the spring-damper system between the car body mass and the bogie element. The midpoint displacements for each model and the difference between the models is illustrated in Figure 3-4.

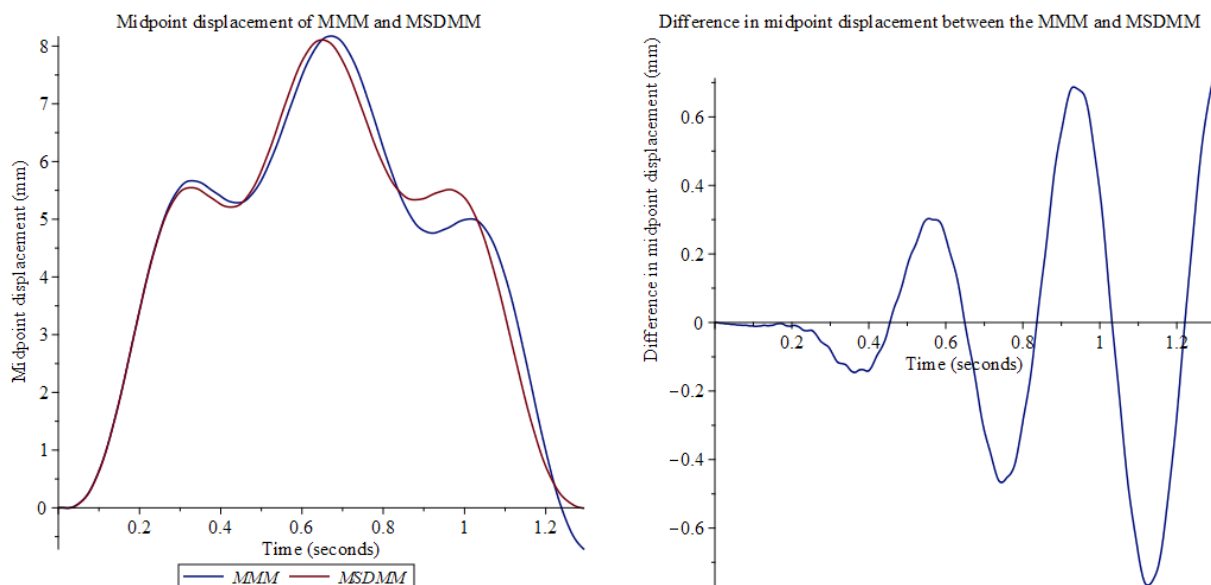


Figure 3-4: Comparison between the MMM and MSDMM results. Midpoint displacements (right) and difference in midpoint displacement (left).

As expected, the left image in Figure 3-4 illustrates that the general trajectories of the midpoint displacement for the MMM and MSDMM are similar.

The right image in Figure 3-4 shows that the difference in midpoint displacement between the two models becomes more extreme as the trains move over the beams. It can be explained through the dynamic interaction between the car body and bogies in the MSDMM model. Figure 3-5 shows the elongation of the spring-damper system between the bogies and the car body.

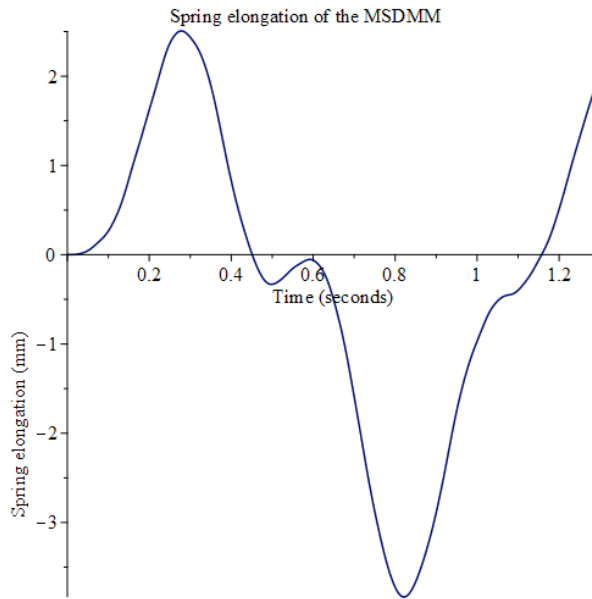


Figure 3-5: Spring elongation of the MSDMM

### 3.3.3 MSDMM vs TAVBM

Upon comparing the simulation results of the MSDMM and the TAVBM, it should be kept in mind that the two models differ in physical size. Whereas the MSDMM consist of only one contact point between the train model and the beam, the TAVBM consists of two contact points with a distance  $d$  between them, corresponding with the distance between bogies.

Figure 3-6 compares the midpoint displacements of the MSDMM and the TAVBM using two different  $x$ -axes. The left image has the time in seconds:  $t = 0$  when the first contact mass enter the beam and the time ends when the model leaves has fully left the beam. The difference in ending time is due physical size difference between the two models.

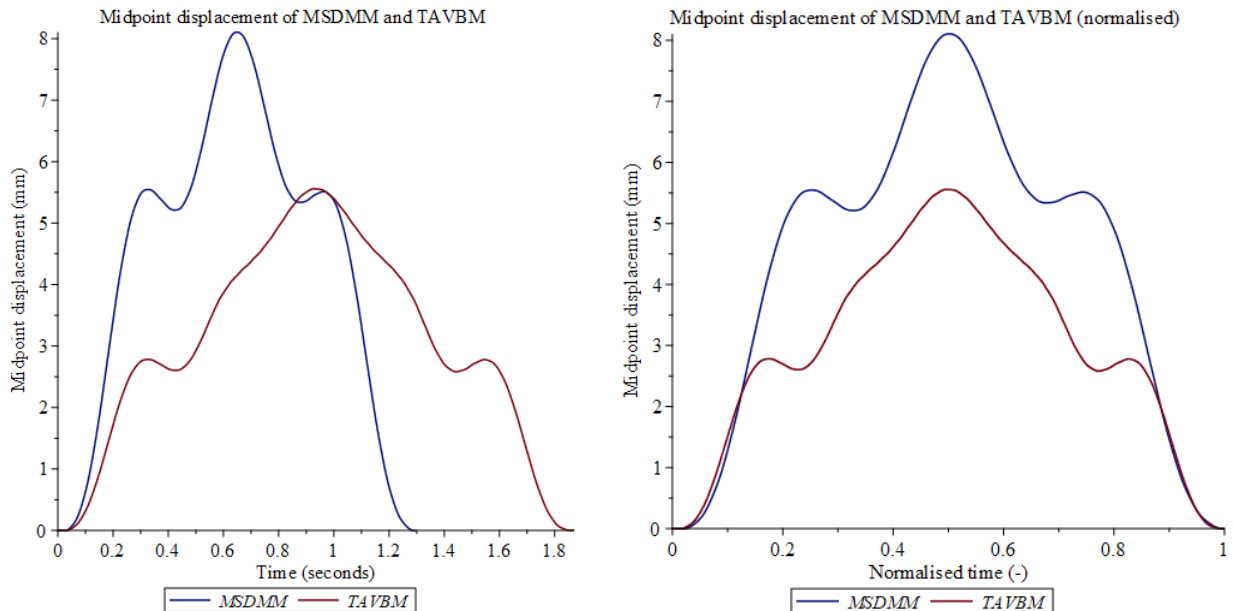


Figure 3-6: Comparison between the MSDMM and TAVBM results. Non-normalised (left) and normalised (right).

Figure 3-6 clearly illustrates a difference in both the trajectory and the maximum of the midpoint displacement. The TAVBM displacement is clearly lower than that of the MSDMM displacement. This is

due to the distribution of forces in the different models: in the MSDMM, all forces are concentrated in one contact point. In the TAVBM the forces are distributed over the beam through 2 different contact points. As a result, the beam displacement is not as significant.

The assumption that the inter-bogie distance  $d$  is the reason for this difference in displacement can be confirmed by simulating the TAVBM using different values for the inter-bogie distance  $d$ . As expected, the TAVBM simulation approaches the MSDMM simulation as  $d$  approaches zero (Figure 3-7).

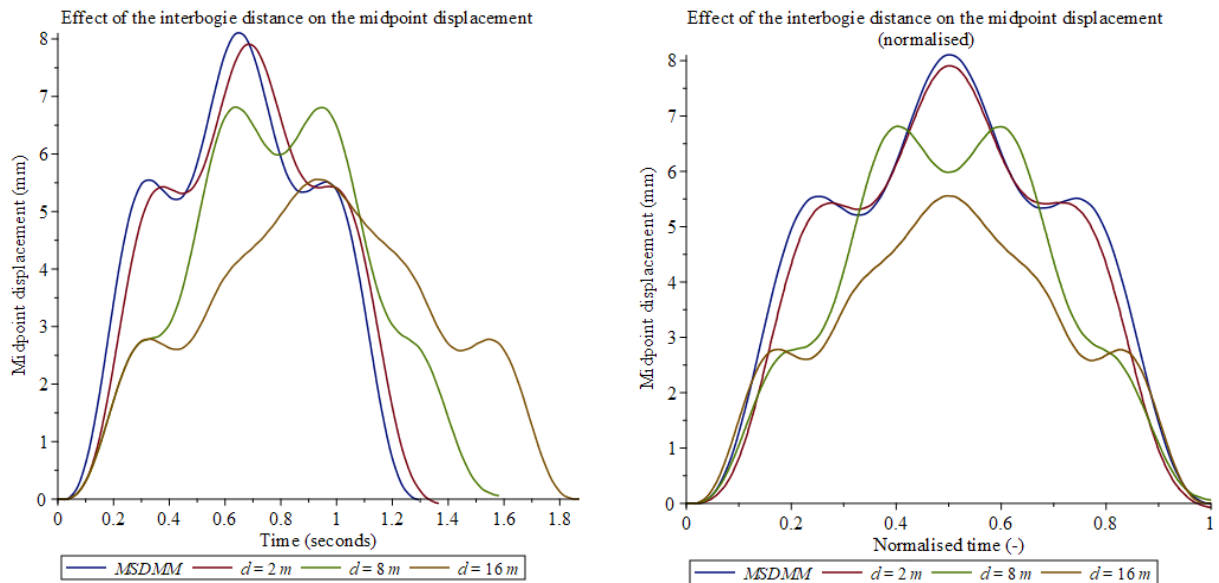


Figure 3-7: Effect of the inter-bogie distance on the midpoint displacement. Non-normalised (left) and normalised (right).

### 3.3.4 TAVBM vs. TBDIM

Between the TAVBM and the TBDIM there is one difference: the wheelsets are considered as separate elements from the bogies. As a result, the bogie-wheelset dynamic interaction is considered in this model which is coupled through the primary suspension of the train.

The comparison between the two models is displayed in Figure 3-8. Like the comparison made in Chapter 3.3.3, the two models differ in physical size; this is due to the additional inter-wheelset distance which is considered. As a result, the simulations cannot be compared directly, and the solutions must be time-normalised as done in the right image of Figure 3-8.

From the comparison it is clear that the results are relatively similar to one another. The slightly different trajectory is attributed to the pitch of the bogies and the introduction of the primary suspension.

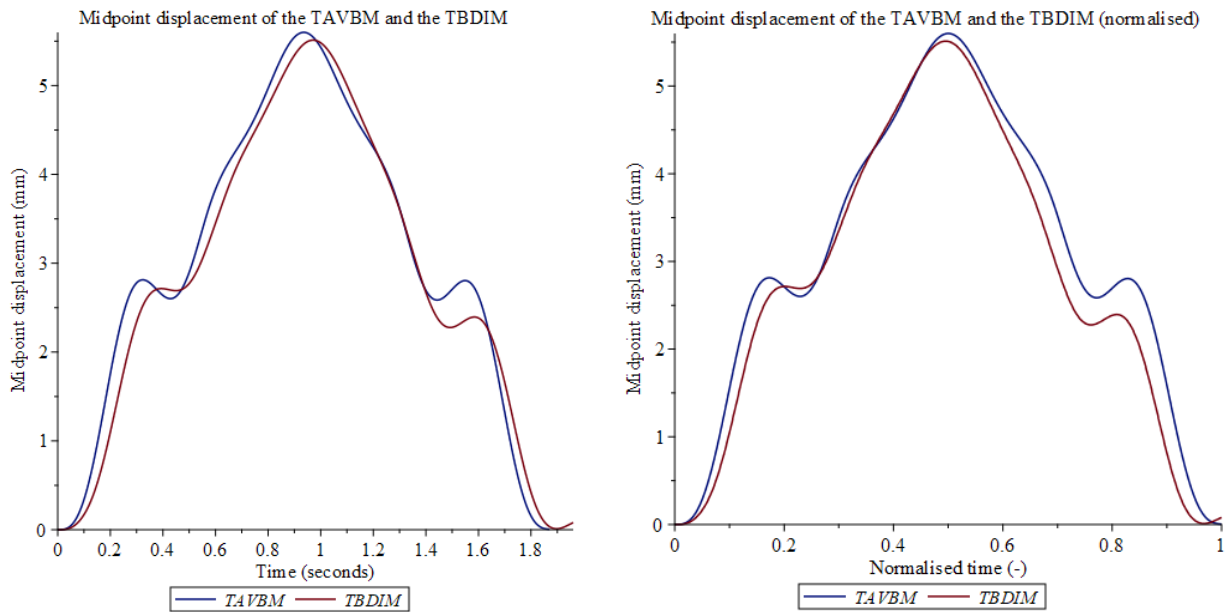


Figure 3-8: Comparison between the TAVBM and TBDIM results. Non-normalised (left) and normalised (right).

### 3.4 Effect of train parameters

For all the modelling results in which the effects of the parameters are analysed, the TBDIM is used. This is because it is the most detailed and accurate model worked out in this research. In contrast to the other models that are calculated, the TBDIM takes both the dynamic interaction between the car body and the bogies and the dynamic interaction between the bogies and wheelsets into account.

#### 3.4.1 Effect of the vehicle speed

Using the TBDIM, simulations are run for different speeds. Figure 3-9 displays the results in 2 different formats: on the left, the time is on the  $x$ -axis. Since the different simulations have varying speeds, they end at different times. As a result, it is difficult to compare the displacements.

On the right, the  $x$ -axis has been time-normalised such that the range of  $x$ -values is the same for all speeds.

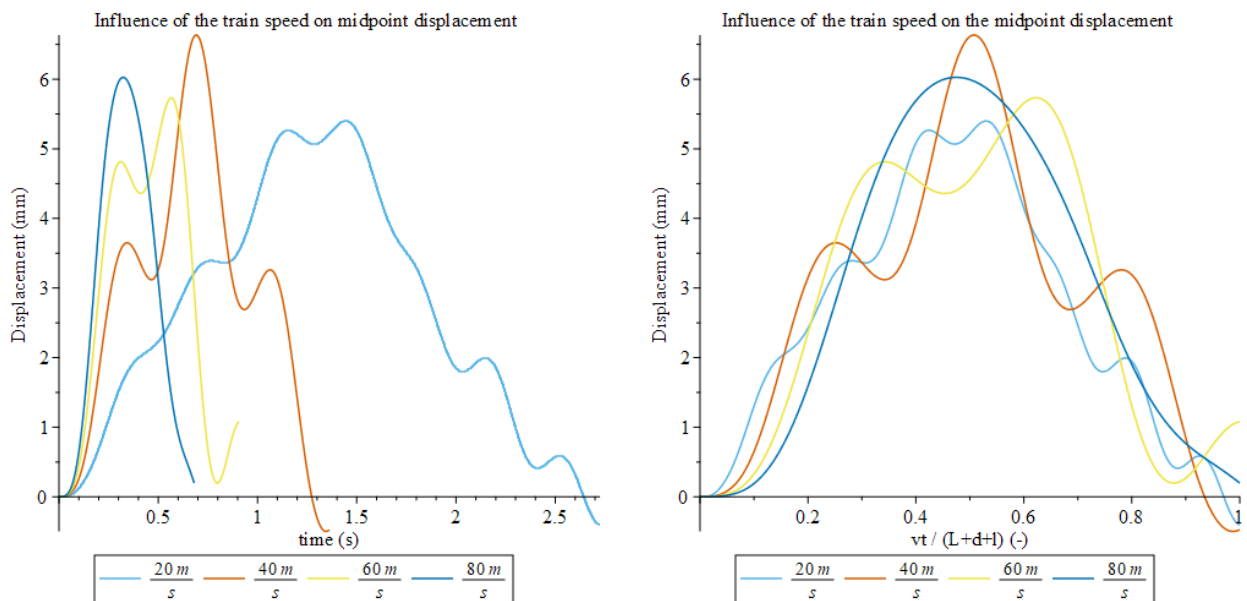


Figure 3-9: Influence of the vehicle speed on the midpoint displacement, non-normalized (left) and normalized (right)

The left image of Figure 3-8 illustrates that the frequency of the harmonic fluctuations in the midpoint displacement is similar between the different vehicle speeds. Because of the difference in total loading duration of the simulations, the number of harmonic fluctuations differs, as shown in the right image of Figure 3-8.

From the right image in Figure 3-9, it can furthermore be concluded that the train velocity does not have a significant effect on the maximum midpoint displacement. This can be attributed to the ‘static solution’ of the models which is the solution if the vehicle dynamics are ignored.

### 3.4.2 Effect of the vehicle mass

Upon analysing the effect of the train mass on the bridge dynamics, only the car body mass is changed. This is because it is the largest mass by a significant margin and is therefore has the most significant effect on the bridge dynamics.

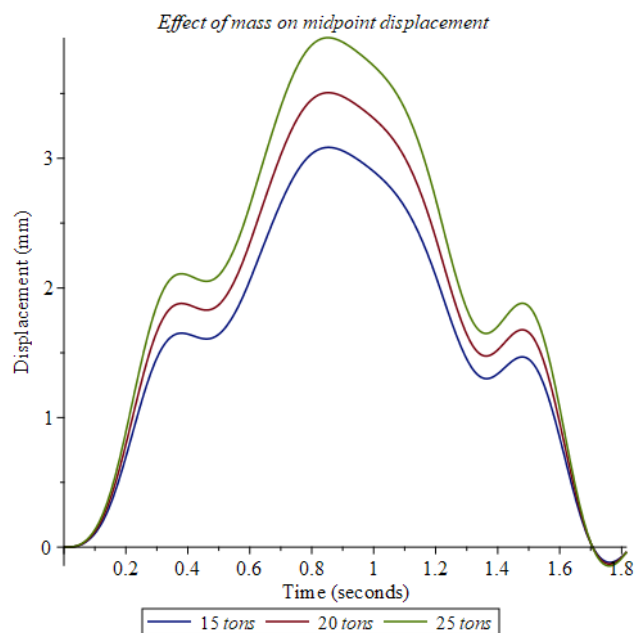


Figure 3-10: Effects of the car body mass on the midpoint displacement

The results in Figure 3-10 show that the midpoint displacement is clearly positively correlated with the car body mass. From the results, the midpoint displacement seems to be directly linearly correlated with the car body mass.

In contrast to the effect on the midpoint displacement, the effect of the car body mass on its own displacement is not as straightforward. From Figure 3-11 it appears that the increase in car body mass appears to extremify the displacements of the car body.

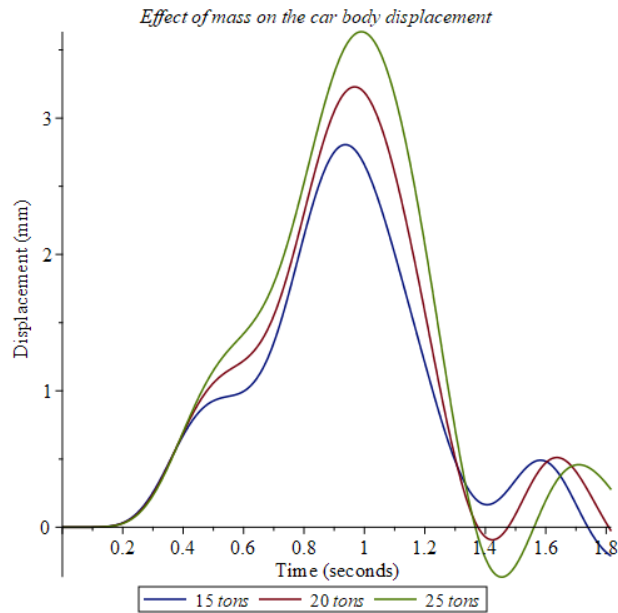


Figure 3-11: Influence of the car body mass on the car body displacement

### 3.4.3 Effect of the suspension parameters

To estimate the effect of the spring stiffness on the midpoint displacement of the beam, the stiffness and damping coefficient of the secondary suspension are changed. In these simulations, the secondary stiffness and secondary damping coefficient are varied by  $\pm 50\%$  from the spring stiffness and damping coefficient as given in Table 2.

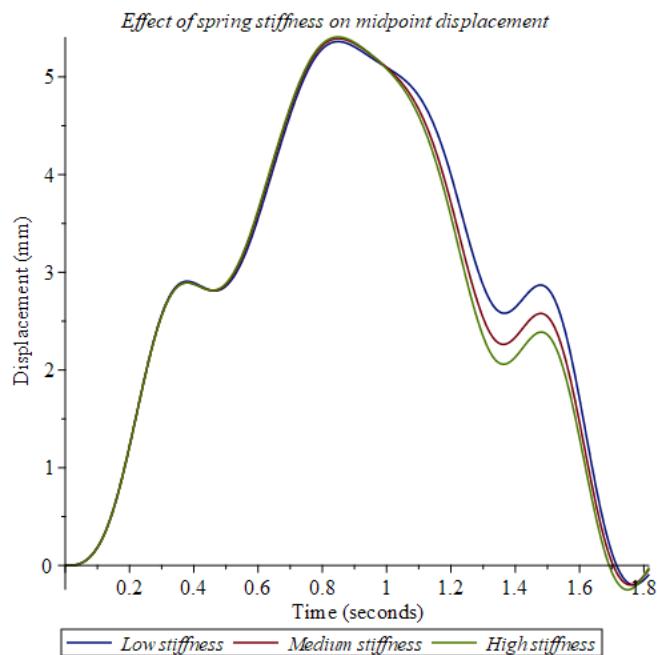


Figure 3-12: Effects of the spring stiffnesses on the midpoint displacement

As can be seen from Figure 3-12, the spring stiffness and damping coefficient of the secondary suspension do not have a significant effect on the midpoint displacement of the beam.

One should note, though, that the difference between the simulations becomes more significant as the train moves along the beam. The absolute difference from the medium stiffness (the real stiffness) to the low and high stiffness are visualised in Figure 3-13.

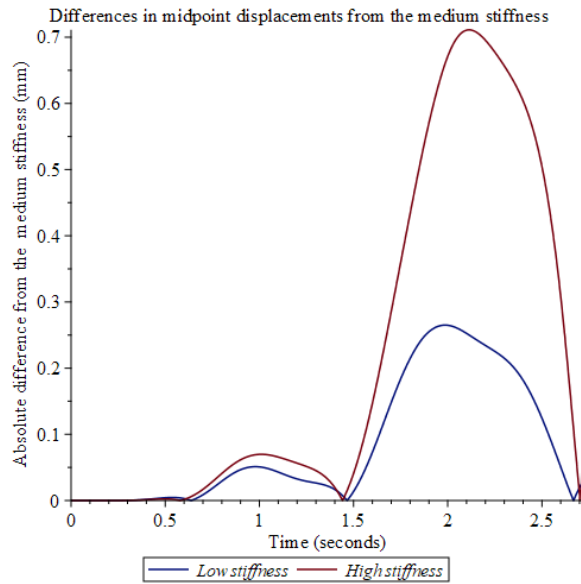


Figure 3-13: Absolute difference from the high and low stiffness simulations to the real stiffness.

From Figure 3-13 it can also be concluded that the stiffness-midpoint displacement relationship is not as simple as the mass-midpoint displacement relationship as described in Chapter 3.4.2. This was expected, as the suspension parameters do not have a direct effect on the beam forcing but dictate the complex dynamic interactions between the bogies and the car body of the train.

The effect of the stiffness of the secondary suspension has a significant effect on the displacement of the car body. As expected, the car body displacement is more significant for lower spring stiffnesses and damping coefficients (Figure 3-14).

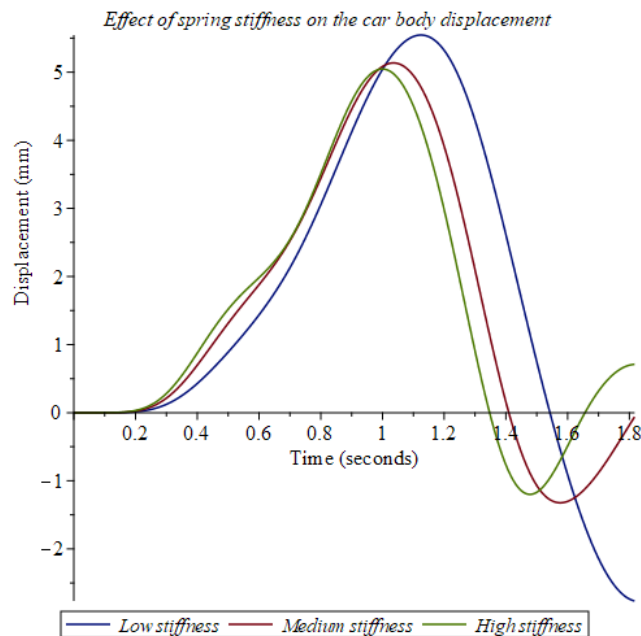


Figure 3-14: Effects of the spring stiffness on the displacement of the car body

#### *4. Conclusions and Discussions*

By fully working out a multitude of train-bridge interaction models, the complexity has been clearly outlined. The complexity of the models gradually increases from the moving force models (MCFM and MHFM) to the TAVBM. Since the solving method of the TBDIM is comparable to that of the TAVBM, the difference in complexity between the TAVBM and TBDIM is insignificant.

The most significant jump in complexity stems from the inclusion of inertia of the train model between the moving force models and the MMM. This difference causes the beam modes to become coupled through the equations for the generalised coordinates. The coupling introduces complications numerical solving method.

Due to the physical shape difference between some of the models, the difference in accuracy cannot be evaluated across all models. Further research must be performed into different models that are of the same physical shape.

The effect of the car body mass on the midpoint displacement is as expected. The apparent direct correlation between the car body mass and the midpoint displacement is in accordance with the use of the weight component in the TBDIM.

There limitations of this study consist of few simplifications that affect the accuracy of the results. Firstly, the wheel/track irregularities were ignored. These irregularities introduce high-frequency dynamics which are not considered in this research. Secondly, the tracks are not considered as separate elements to the bridge. This would introduce further complexity coupled with a higher accuracy.

Thirdly, the track-bridge was modelled as a Euler-Bernoulli beam. As explained in Chapter 2.1, this simplification ignores the effects of shear deformation and rotational bending. To obtain more accurate results (with a higher complexity) a more detailed beam theory should be used such as the Timoshenko–Ehrenfest beam. Lastly, this research only investigates the passing of a train over a bridge of a single span.

For further research I would recommend investigating the effects of bridge parameters on the train-bridge dynamic interaction. Furthermore, in the light of passenger comfort, the effect of the model complexity on the accuracy of the car body acceleration should be determined.

Furthermore, to thoroughly investigate the effects of the dynamics of the train on the bridge dynamics, further modelling should be performed using series of point loads instead of a single point load as is done in this research.

## References

- Andersson, A., & Karoumi, R. (2015). Dynamics of railway bridges, analysis and verification by field tests. *6th International Conference on Experimental Vibration Analysis for Civil Engineering Structures*. EDP Sciences. Retrieved from [matec-conferences.org/articles/mateconf/pdf/2015/05/mateconf\\_evaces2015\\_01001.pdf](http://matec-conferences.org/articles/mateconf/pdf/2015/05/mateconf_evaces2015_01001.pdf)
- Biggs, J. M. (1964). *Introduction to structural dynamics*. Massachusetts: McGraw-Hill Book Company.
- Cantero, D., Karoumi, R., & Ülker-Kaustell, M. (2016, February). Time-frequency analysis of railway bridge response in forced vibration. *Mechanical Systems and Signal Processing*. Retrieved from <http://dx.doi.org/10.1016/j.ymssp.2016.01.016>
- Chen, Z., & Han, Z. (2017). Dynamic Analysis of High-Speed Train-Track-Bridge Coupled System Considering Concrete Shrinkage and Creep. *First International Conference on Rail Transportation 2017*. Chengdu.
- Devesa, J. (2009). Influence of Soil Stiffness on the Dynamic Behaviour of Bridges Traveled by High Speed Trains. *Structural Engineering International: Journal of the International Association for Bridge and Structural Engineering*, 383–394. Retrieved from <https://doi.org/10.2749/101686609789847028>
- Erochko, J. (2020). *5.2 The Bernoulli-Euler Beam Theory*. Retrieved from Learn About Structures: <https://learnaboutstructures.com/Bernoulli-Euler-Beam-Theory>
- Eurostat. (2020). Railway passenger transport statistics - quarterly and annual data. *Eurostat statistics explained*. Retrieved from [https://ec.europa.eu/eurostat/statistics-explained/index.php?title=Railway\\_passenger\\_transport\\_statistics\\_-\\_quarterly\\_and\\_annual\\_data](https://ec.europa.eu/eurostat/statistics-explained/index.php?title=Railway_passenger_transport_statistics_-_quarterly_and_annual_data)
- Frýba, L. (1972). *Vibration of Solids and Structures under Moving Loads*. Prague: ThomasTelford.
- Jalili, M., & Orafa, A. (2014). A dynamic model for the interaction of the cable bridge and train system. *International Journal of Civil Engineering*. Retrieved from [http://ijce.iust.ac.ir/files/site1/user\\_files\\_6k93w6/mjalili-A-10-1654-1-7f5e0b4.pdf](http://ijce.iust.ac.ir/files/site1/user_files_6k93w6/mjalili-A-10-1654-1-7f5e0b4.pdf)
- Jeffcot, H. (1929). VI. On the vibration of beams under the action of moving loads. *The London, Edinburgh, and Dublin Philosophical Magazine and Journal of Science*, 66-97.
- Kolousek, V. (1973). *Dynamics in Engineering Structures*. London: Butterworths.
- Li, X.-Z., Liu, X.-H., Liu, D.-J., & Zhang, X. (2013). Influences of Soil-Structure Interaction on Coupled Vibration of Train-Bridge System: Theoretical and Experimental Study. *Advances in Structural Engineering*, 1355-1364. Retrieved from <https://doi.org/10.1260/1369-4332.16.8.1355>
- Ling, L., Dhanasekar, M., & Thambiratnam, D. P. (2017). Dynamic response of the train-track-bridge system subjected to derailment impacts. *International Journal of Vehicle Mechanics and Mobility*, 638-657. Retrieved from <https://doi.org/10.1080/00423114.2017.1398341>
- Lorieux, L. (2008). Analysis of train-induced vibrations on a single-span composite bridge. *TRITA-BKN*. Retrieved from <https://www.diva-portal.org/smash/get/diva2:431850/FULLTEXT01.pdf>
- Maghdid, D. (2002). *Stability and accuracy of Newmark's method*. doi:<http://dx.doi.org/10.13140/RG.2.1.3918.3760>

- Majka, M., & Hartnett, M. (2008). Effects of speed, load and damping on the dynamic response of railway bridges and vehicles. *Computers & Structures*, 556-572. Retrieved from <https://doi.org/10.1016/j.compstruc.2007.05.002>
- Newmark, N. M., & Chan, S. P. (1952). *A comparison of Numerical Methods for Analyzing the Dynamic Response of Structures*. Urbana: University of Illinois. Retrieved from [https://www.researchgate.net/profile/Debasish-Mondal-8/post/What\\_is\\_the\\_advantage\\_of\\_Newmark\\_method\\_over\\_Runge-kutta\\_method\\_when\\_it\\_comes\\_to\\_Structural\\_dynamics/attachment/59d6545779197b80779abc8/AS%3A521314570326016%401501302487837/download/A+Comparison](https://www.researchgate.net/profile/Debasish-Mondal-8/post/What_is_the_advantage_of_Newmark_method_over_Runge-kutta_method_when_it_comes_to_Structural_dynamics/attachment/59d6545779197b80779abc8/AS%3A521314570326016%401501302487837/download/A+Comparison)
- Sneideris, J., Bucinska, P., Agapii, L., & Andersen, L. (2015). Experimental Validation of a Numerical Model for Three-Dimensional High-Speed Railway Bridge Analysis by Comparison with a Small-Scale Model. *Fifteenth International Conference on Civil, Structural and Environmental Engineering Computing*. Stirlingshire: Civil-Comp Press. Retrieved from <https://www.ctresources.info/ccp/paper.html?id=8685>
- Stokes, G. G. (1849). Discussion of a differential equation relating to the breaking of railway bridges. *Transactions of the Cambridge Philosophical Society*. Retrieved from <https://books.google.com/books?id=2vsIAAAIAAJ&pg=PA533>
- Tian, Y., Zhang, N., & Xia, H. (2016). Temperature effect on service performance of high-speed railway concrete bridges. doi:<https://doi.org/10.1177%2F1369433216665306>
- Timoshenko, S. (1922). On the forced vibration of bridges. *The London, Edinburgh, and Dublin Philosophical Magazine and Journal of Science*, 1018-1019.
- Ülker-Kaustell, M., Karoumi, R., & Pacoste, C. (2010). Simplified analysis of the dynamic soil–structure interaction of a portal frame railway bridge. *Engineering Structures*, 3692-3698. Retrieved from <https://doi.org/10.1016/j.engstruct.2010.08.013>
- Wen, R. K. (1960). Dynamic Resposne of Beams Traversed by Two-Axle Loads. *Journal of the Engineering Mechanics Division*.
- Willis, R. (1849). *The effects produced by causing weights to travel over elastic bars*. Cambridge. Retrieved from [http://robertwillis2016.org/Library/pdf/1849\\_Willis\\_An\\_essay\\_on\\_the\\_effects\\_produced\\_by\\_causing\\_weights\\_to\\_travel\\_over\\_elastic\\_bars\\_OCR.pdf](http://robertwillis2016.org/Library/pdf/1849_Willis_An_essay_on_the_effects_produced_by_causing_weights_to_travel_over_elastic_bars_OCR.pdf)
- Wolswijk, W. (2021). *Train Bridge Dynamic Models*. Retrieved from GitHub: <https://github.com/WillemWolswijk/Train-bridge-Dynamic-Models.git>
- Wu, Y.-S., & Yang, Y.-B. (2004). A semi-analytical approach for analyzing ground vibrations caused by trains moving over elevated bridges. *Soil Dynamics and Earthquake Engineering*, 949-962. Retrieved from <https://doi.org/10.1016/j.soildyn.2004.06.020>
- Xia, W. M., & Liu, X. M. (2014). The Response Analysis of the Train-Bridge System under Seismic Action. *Applied Mechanics and Materials*, 587–589. Retrieved from <https://doi.org/10.4028/www.scientific.net/amm.587-589.1443>
- Yang, Y. B., Yau, J. D., & Wu, Y. S. (2004). *Vehicle-Bridge Interaction Dynamics with Applications to High-Speed Railways*. Singapore: World Scientific Publishing Co.

- Zhai, W., & Sun, X. (1994). A Detailed Model for Investigating Vertical Interaction between Railway Vehicle and Track. *International Journal of Vehicle Mechanics and Mobility*, 603-615. Retrieved from <https://doi.org/10.1080/00423119308969544>
- Zhai, W., Han, Z., Chen, Z., Ling, L., & Zhu, S. (2019). Train-track-bridge dynamic interaction: a state-of-the-art review. *International Journal of Vehicle Mechanics and Mobility*. doi:<https://doi.org/10.1080/00423114.2019.1605085>
- Zhang, N., Xia, H., & Guo, W. (2008). Vehicle-bridge interaction analysis under high-speed trains. *Journal of Sound and Vibration*, 407-425. doi:<https://doi.org/10.1016/j.jsv.2007.07.064>
- Zhu, Z. H., Yu, Z. W., Zhu, Y. L., & Gao, M. M. (2013). Analysis on environment and building vibration induced by passing trains on bridge structures. *Tiedao Xuebao/Journal of the China Railway Society*. Retrieved from <https://d.wanfangdata.com.cn/periodical/tdxb201304016>